

Structural precursor to the metal-insulator transition in V_2O_3

P. Pfalzer, G. Obermeier, M. Klemm, and S. Horn

Institut für Physik, Universität Augsburg, Universitätsstraße 1, 86159 Augsburg, Germany

M. L. denBoer

Queens College of CUNY, 65-30 Kissena Blvd., Flushing, New York 11367

(Dated: May 24, 2019)

The temperature dependence of the local structure of V_2O_3 in the vicinity of the metal to insulator transition (MIT) has been investigated using hard X-ray absorption spectroscopy. It is shown that the vanadium pair distance along the hexagonal c -axis changes abruptly at the MIT as expected. The tilt of these pairs, however, sets in at higher temperatures and already has reached its maximum value at the onset of the electronic and magnetic transition. These findings suggest that interactions in the basal plane play a decisive role for the MIT and orbital degrees of freedom drive the MIT via changes in hybridization.

PACS numbers: 71.30.+h, 61.10.Ht, 71.27.+a, 78.70.Dm

The metal to insulator transition in V_2O_3 is a long standing yet not completely resolved issue. Originally being discussed as the classical example of a Mott-Hubbard transition [1], this interpretation has to be questioned due to the intimate interplay of structural, electronic and magnetic changes in the phase diagram of this compound [2]. Therefore it is not clear whether electronic correlations can completely account for the MIT in V_2O_3 or if structural effects play an important role. The relevance of possible electron-lattice interactions has been stressed by recent theoretical work [3, 4].

In an earlier paper [5] we have shown that a detailed understanding of the interplay of structural and electronic degrees of freedom requires both information on the global structure as measured by X-ray diffraction (XRD) and of the local structure of the compound. Interatomic distances and symmetries can deviate locally from the global lattice symmetry, therefore indicating the presence of an order-disorder component of the transitions or of structural fluctuations. Our earlier results demonstrate that the two insulating phases of V_2O_3 , the paramagnetic insulating (PI) and the antiferromagnetic insulating (AFI) phase, are structurally very similar on a local scale and therefore indicate that there might exist a common route for both the transitions from the paramagnetic metallic (PM) phase to the PI and the AFI phase, respectively.

In this letter, we investigate the evolution of the local structure of V_2O_3 in the vicinity of the PM to AFI transition to shed light on the detailed structural changes associated with the MIT. The results of our temperature dependent extended X-ray absorption fine structure (EXAFS) measurements show a rather complex behavior of the local structure, which differs along different crystallographic axes. In particular, we observe a structural precursor to the MIT which consists of characteristic changes of nearest neighbor distances for the first time.

EXAFS measurements were performed on a V_2O_3 single crystal grown by chemical transport using TeCl_4 as transport agent. The crystal was mounted on a thin glass plate and reduced in thickness by lapping and polishing the sample down to approximately $12\ \mu\text{m}$ which corresponds to roughly two absorption lengths. This treatment allowed to detect the X-ray absorption in a transmission geometry, thereby avoiding damping of the signal due to selfabsorption effects which would have been present in fluorescence mode [6]. The sample was oriented so that the angle between the polarization vector \mathbf{E} of the incoming X-rays and the hexagonal c axis (\mathbf{c}_{hex}) could be changed by rotating the sample around the surface normal. Measurements were made with \mathbf{E} parallel and perpendicular to \mathbf{c}_{hex} . This procedure allows to separate scattering paths along and perpendicular to the hexagonal c axis [5]. The electrical resistivity was measured using a standard four-probe DC technique. For each measurement the current was reversed to eliminate offsets. Metallic behavior was observed in the high temperature region, and a sharp jump in the resistance of more than three orders of magnitude at a temperature of 140 K signaled the MIT [7]. The slightly reduced transition temperature indicates that a small vanadium deficiency occurred during the growth of the single crystal. The magnetic transition from PM to AFI occurred in a temperature region from 140 K down to 130 K as determined by magnetic susceptibility measurements using a Quantum Design superconducting quantum interference device (SQUID) magnetometer.

EXAFS measurements at the vanadium K edge (5465 eV) were performed at beam line X23B of the National Synchrotron Light Source at Brookhaven National Laboratory. Spectra at different temperatures above, at, and below the transition temperature were taken using a closed cycle helium cryostat. The sample was held under vacuum to avoid water condensation and to reduce heat transmission. As no temperature sensor was available in

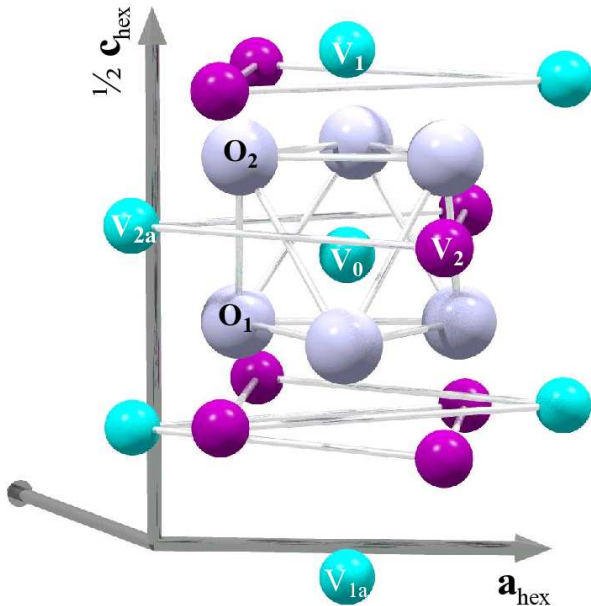


FIG. 1: (color online). Room temperature structure of V_2O_3 . Small (large) spheres represent vanadium (oxygen) ions. Only those oxygen ions which form an octahedron around the central vanadium ion V_0 are shown. Vanadium ions which have opposite spin in the AFI phase are drawn in different colors.

the direct neighborhood of the sample, the resistivity of the crystal was monitored *in situ* during the EXAFS experiment in the geometry with \mathbf{E} perpendicular to \mathbf{c}_{hex} . The electronic transition was observed at a temperature of 130 K at the cold finger of the cryostat. The temperature difference of -10 K compared to the *ex situ* resistance measurements can be attributed to a temperature gradient between the cold finger and the sample. Temperatures given in the paper are corrected accordingly. EXAFS spectra above the transition were measured before and after the crystal passed through the MIT. No differences were observed, ruling out the influence of possible cracks on the measurements.

Standard EXAFS analysis using the ATHENA [8] and IFEFFIT [9] programs was performed to extract path lengths and other parameters from the spectra. For the Fourier transforms a window in k space from 2 \AA^{-1} to 13 \AA^{-1} was used (k being the wavevector of the photo-electron) and the spectra were weighted by $k^{2.5}$. Model spectra calculated with FFF8.2 [10] were fitted to the measured spectra in real space in a range from 1.2 \AA to 4.1 \AA ($\mathbf{E} \parallel \mathbf{c}_{\text{hex}}$) and from 1.2 \AA to 3.65 \AA ($\mathbf{E} \perp \mathbf{c}_{\text{hex}}$), respectively. The cluster of ions used for the calculations of the model spectra was derived from the lattice parameters and atomic positions resulting from XRD measurements for the trigonal structure of V_2O_3 at room temperature published in Ref. 11.

The structure refinement was performed by varying the interatomic distances to all vanadium ions up to a shell

radius of 4.3 \AA , which corresponds to the V ions shown in Fig. 1. In addition, backscattering from the six oxygen ions that form the coordination octahedron of the absorber was accounted for. Inclusion of the second backscattering shell of oxygen ions improved the quality of the fit, but had no influence on the fitting parameters concerning the ions shown in Fig. 1. At the transition from the paramagnetic metal to the antiferromagnetic insulator, the lattice symmetry reduces from trigonal to monoclinic. Comparing the interatomic distances of the trigonal and the monoclinic structure as calculated from the data published in Refs. 11 and 12, 13, 14 it turns out that the transition increases the distance of the neighboring vanadium ions along the hexagonal c axis (V_0 and V_1) by 0.04 \AA . In addition, the threefold symmetry in the plane perpendicular to \mathbf{c}_{hex} (the basal plane) is broken and one of the three vanadium neighbors in this plane (V_{2a}) increases its distance to the absorber (V_0) by 0.11 \AA , while the distance to the two other V_2 ions remains nearly constant. To allow for this monoclinic distortion in the fitting model, the distance between the absorber and these V neighbors (V_1 for the spectra with $\mathbf{E} \parallel \mathbf{c}_{\text{hex}}$ and V_{2a} for the spectra with $\mathbf{E} \perp \mathbf{c}_{\text{hex}}$) was allowed to vary freely, while the distances to the remaining V and O ions were given as multiples of this value. For the oxygen ions an additional isotropic change of the distances was allowed. A damping term (Debye-Waller factor) was assigned to each neighboring shell, and for the nearest vanadium neighbors the third cumulant was used as an additional free parameter.

All measured spectra could be fitted successfully with a reliability factor of less than 0.02, indicating that the model was well suited to describe the data. Figures 2 and 3 show the fit results for the scattering paths to the next vanadium neighbors along (V_1) and perpendicular (V_2 , V_{2a}) to the hexagonal c axis. The geometry used in the measurement allowed for a separation of these paths: Backscattering from the V_1 neighbor only occurs in the spectra with $\mathbf{E} \parallel \mathbf{c}_{\text{hex}}$, while the V_2 and V_{2a} backscatters only contribute to the spectra with $\mathbf{E} \perp \mathbf{c}_{\text{hex}}$. The Fourier transformed spectra show a well separated structure located between 2 \AA and 3 \AA . This structure is attributed to single scattering contributions either of the V_1 or the V_2 , V_{2a} scattering paths, only. Therefore no correlations between fit variables of these paths can occur, although the distance from the absorber V_0 to all of these neighbors is similar.

Figure 2(a) clearly shows that the distances between the next V neighbors along the hexagonal c axis correspond to the values expected from XRD results: The distance in the AFI phase at low temperatures is about 0.04 \AA larger than in the high temperature PM phase. The change is abrupt as a function of temperature and occurs in a temperature window corresponding to that of the change in magnetic susceptibility. The measurement uncertainty of

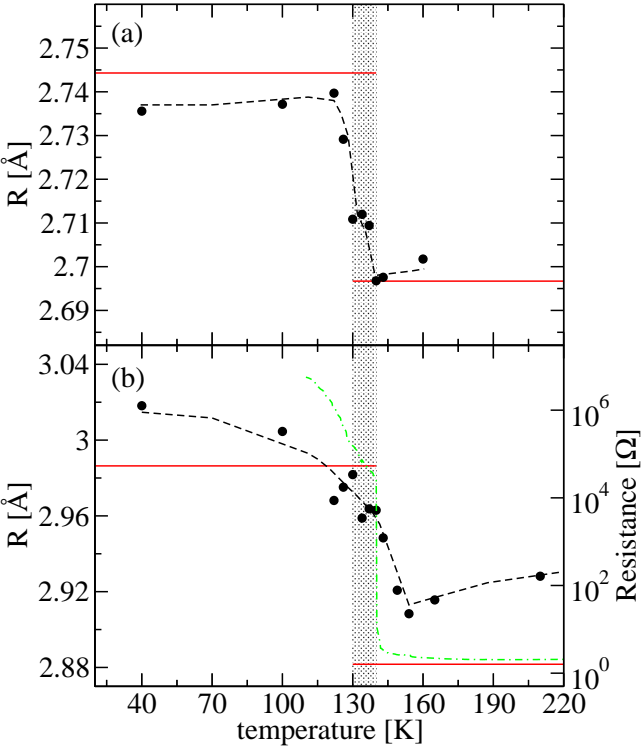


FIG. 2: (color online). Temperature dependence of the distances of the V_0 – V_1 (a) and V_0 – V_{2a} (b) scattering paths as resulting from the fits to the EXAFS spectra (dots). Solid lines represent the distances expected from XRD. The dash-dotted line in (b) shows the result of the *ex situ* resistance measurement. The shaded temperature range marks the range of the magnetic transition. Dashed lines through the fit results provide a guide to the eye.

the V_0 – V_1 distances amounts to ≈ 0.01 Å. The Debye-Waller factor σ^2 , shown in Fig. 3(a), exhibits a sharp rise at the onset of the MIT, indicating either large fluctuations or a static distribution of widely varying distances while the magnetic transition occurs.

The next neighbor distances in the basal plane display a very different behavior. First of all the distance from the absorber ion V_0 to the V_{2a} neighbor is larger than expected from XRD in the high temperature PM phase [see Fig. 2(b)], i.e. larger than the V_0 – V_2 distances. This break of the threefold symmetry expected from the long range structure probed by XRD corresponds to a monoclinic symmetry. The elongation of the V_0 – V_{2a} distance, which could be determined with an accuracy of ≈ 0.02 Å, measures the size of this monoclinic distortion. In the PM phase it is reduced to about 30 % of the distortion in the AFI phase, as was first observed in Ref. 15. The transition to the full monoclinic distortion in the basal plane is much broader in temperature than that observed for the V-V distance along the hexagonal c axis. The onset occurs in a region well above the electronic and magnetic transitions. This is consistent with the fact that

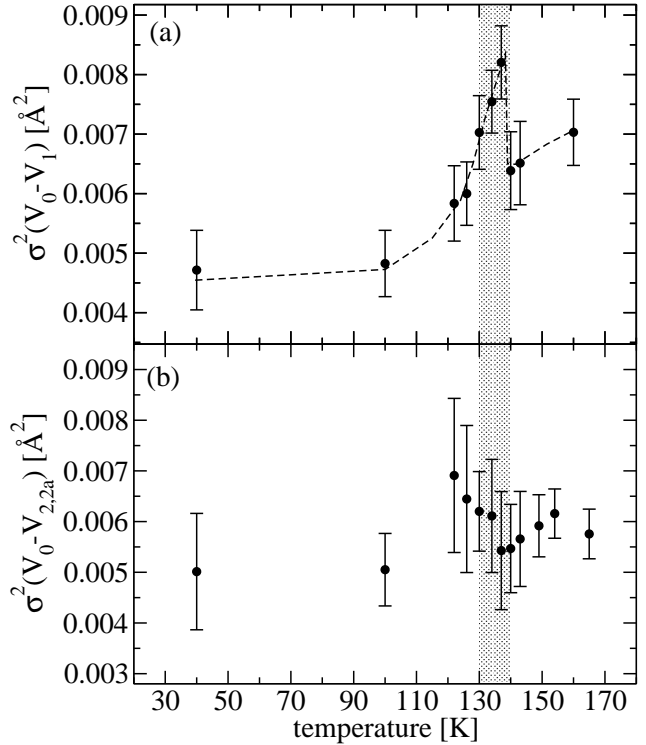


FIG. 3: Temperature dependence of the Debye-Waller factors σ^2 for the V_0 – V_1 (a) and V_0 – $V_{2,2a}$ (b) scattering paths as resulting from the fits to the EXAFS spectra. Like in Fig. 2, the shaded temperature range marks the range of the magnetic transition. The dashed line through the fit results provides a guide to the eye.

the Debye-Waller factor of the in-plane V neighbors [Fig. 3(b)] does not show a significant change at the MIT.

Third cumulants ($\sigma^{(3)}$) which account for the anisotropy of the scattering paths to the next V neighbors were found to have a significant influence on the spectra in the low temperature AFI phase, but are negligible in the PM phase. The third cumulants show only a weak temperature dependence in the AFI phase and adopt values of ≈ -0.0003 Å³ for the V_0 – V_1 scattering path and ≈ -0.0007 Å³ for the V_0 – V_2 and V_0 – V_{2a} scattering paths, respectively. The error is estimated to approximately ± 25 %.

Summarizing, we can characterize the structural evolution at the metal to insulator transition of V_2O_3 as follows: Structural changes along the hexagonal c axis are restricted to a sharply bounded temperature range given by the MIT. Perpendicular to c_{hex} , however, the tilt of the c -axis V pairs, indicated by the elongation of the V_0 – V_{2a} bond, starts to increase already far above the MIT.

Precursor effects to the MIT in V_2O_3 have already been observed in electrical resistance under pressure [16] and very recently in the sound velocity measured for thin films [17]. The results of our local structure determination show for the first time that structural changes

precede the changes in transport and magnetic properties.

Following Tanaka [3], hybridization between the a_{1g} and the e_g^π orbitals increases on rotating the V_0 – V_1 pairs out of the direction of the c -axis. The so modified interactions favor a new ground state configuration with a reduced occupation of the a_{1g} orbital [18]. In this configuration, the electron-lattice coupling is strong and an enlarged V pair distance is expected. Therefore it is plausible that the V_0 – V_1 distance expands primarily after the tilt of the pair has adopted its maximum value. The fact, that on a local scale the trigonal symmetry is not fully recovered in the metallic phase, suggests that the trigonal and monoclinic structure are very close in energy, allowing fluctuations between the two. We want to point out that the present results are consistent with our earlier findings [5] that the trigonal symmetry can be broken on a local scale while the global symmetry remains trigonal. In step with the separation of the two neighboring V ions along the hexagonal c axis an “umbrella like” distortion of the oxygen coordination octahedron around each V ion occurs [19]. The increased distortion of the oxygen octahedron is responsible for the stabilization of the insulating state [4] since it results in a large shift of (dynamical) spectral weight.

However, from theoretical considerations it has been pointed out [20] that in-plane interactions are important for the MIT in V_2O_3 and should not be treated as small perturbations. This view is supported by our measurements which suggest that in-plane interactions are a decisive ingredient to the MIT by triggering the modification of the V_0 – V_1 distance via changes in hybridization. In this context it is interesting to note that the Debye-Waller factor of the in-plane vanadium neighbors does not display substantial changes at the transition. If structural degrees of freedom were the driving force behind the increase of the in-plane interatomic distances, the Debye-Waller factor should be strongly affected. A possible explanation could be that the change in hybridization is driven by orbital interactions. The change in hybridization will also result in a change of the crystal field splitting and accordingly alter the orbital occupation. Evidence for orbital interactions is given from neutron scattering results by Bao *et al.* [21]. As shown by Laad *et al.*, the variation of orbital occupation can result in a first order phase transition [22].

In conclusion, the measurements of the local structure of pure V_2O_3 in the vicinity of the metal to insulator transition show that complex changes of the interatomic distances on a local scale are decisive for the changes of the physical properties at the transition. At the onset of the electronic and magnetic transition temperature, the next vanadium neighbors along the hexagonal c axis increase their distance, resulting in an increase of the trigonal crystal field component and a shift of spectral weight, rendering the system insulating. However, an increase of

the monoclinic distortion in the basal plane is already observed far above the MIT reaching its maximum value at the onset of the electronic and magnetic transition. These findings suggest that the metal to insulator transition could be driven by changes in the hybridization triggered by in-plane orbital interactions.

We appreciate valuable assistance in the measurements from J. Kirkland at NSLS. This work was supported by the DFG through SFB 484. The NSLS is supported by the DOE.

- [1] D. B. McWhan, T. M. Rice, and J. P. Remeika, *Phys. Rev. Lett.* **23**, 1384 (1969).
- [2] D. B. McWhan, A. Menth, J. P. Remeika, W. F. Brinkman, and T. M. Rice, *Phys. Rev. B* **7**, 1920 (1973).
- [3] A. Tanaka, *J. Phys. Soc. Jpn.* **71**, 1091 (2002).
- [4] M. S. Laad, L. Craco, and E. Müller-Hartmann, *cond-mat/0505317*.
- [5] P. Pfalzer, J. Will, A. Nateprov, Jr., M. Klemm, V. Eyert, S. Horn, A. I. Frenkel, S. Calvin, and M. L. denBoer, *Phys. Rev. B* **66**, 085119 (2002).
- [6] P. Pfalzer, J.-P. Urbach, M. Klemm, S. Horn, M. L. denBoer, A. I. Frenkel, and J. P. Kirkland, *Phys. Rev. B* **60**, 9335 (1999).
- [7] All temperatures given in this letter are measured on cooling.
- [8] B. Ravel and M. Newville, *J. Synchrotron Rad.* **12**, 537 (2005).
- [9] M. Newville, *J. Synchrotron Rad.* **8**, 322 (2001).
- [10] A. L. Ankudinov, C. E. Bouldin, J. J. Rehr, J. Sims, and H. Hung, *Phys. Rev. B* **65**, 104107 (2002).
- [11] M. G. Vincent, K. Yvon, and J. Ashkenazi, *Acta Crystallogr. Sect. A* **36A**, 808 (1980).
- [12] D. B. McWhan and J. P. Remeika, *Phys. Rev. B* **2**, 3734 (1970).
- [13] P. D. Dernier and M. Marezio, *Phys. Rev. B* **2**, 3771 (1970).
- [14] L. D. Calvert and P. Villars, *Pearson's Handbook of Crystallographic Data for Intermetallic Phases*, vol. 4 (ASM international, 1991).
- [15] A. I. Frenkel, E. A. Stern, and F. A. Chudnovsky, *Solid State Commun.* **102**, 637 (1997).
- [16] S. A. Carter, T. F. Rosenbaum, M. Lu, H. M. Jaeger, P. Metcalf, J. M. Honig, and J. Spalek, *Phys. Rev. B* **49**, 7898 (1994).
- [17] C. Müller, A. A. Nateprov, G. Obermeier, M. Klemm, R. Tidecks, A. Wixforth, and S. Horn, *cond-mat/0506702*.
- [18] J. H. Park, L. H. Tjeng, A. Tanaka, J. W. Allen, C. T. Chen, P. Metcalf, J. M. Honig, F. M. F. de Groot, and G. A. Sawatzky, *Phys. Rev. B* **61**, 11506 (2000).
- [19] P. D. Dernier, *J. Phys. Chem. Solids* **31**, 2569 (1970).
- [20] I. S. Elfimov, T. Saha-Dasgupta, and M. A. Korotin, *Phys. Rev. B* **68**, 113105 (2003).
- [21] W. Bao, C. Broholm, G. Aeppli, P. Dai, J. M. Honig, and P. Metcalf, *Phys. Rev. Lett.* **78**, 507 (1997).
- [22] M. S. Laad, L. Craco, and E. Müller-Hartmann, *Phys. Rev. Lett.* **91**, 156402 (2003).